Impact of Viscous and Heat Relaxation Loss on the Critical Temperature Gradients of Thermoacoustic Stacks

Zhibin Yu, Artur J. Jaworski, and Abdulrahman S. Abduljalil

Abstract—A stack with a small critical temperature gradient is desirable for a standing wave thermoacoustic engine to obtain a low onset temperature difference (the minimum temperature difference to start engine's self-oscillation). The viscous and heat relaxation loss in the stack determines the critical temperature gradient. In this work, a dimensionless critical temperature gradient factor is obtained based on the linear thermoacoustic theory. It is indicated that the impedance determines the proportion between the viscous loss, heat relaxation losses and the power production from the heat energy. It reveals the effects of the channel dimensions, geometrical configuration and the local acoustic impedance on the critical temperature gradient in stacks. The numerical analysis shows that there exists a possible optimum combination of these parameters which leads to the lowest critical temperature gradient. Furthermore, several different geometries have been tested and compared numerically.

Keywords—Critical temperature gradient, heat relaxation, stack, viscous effect.

I. INTRODUCTION

THERMOACOUSTIC energy-conversion devices have attracted researchers' attention in the past decades because of the lack of moving parts, which potentially offers high reliability and low cost. However, thermoacoustic devices have still not achieved the efficiencies as high as those of conventional heat engines. For standing wave thermoacoustic engines [1], the thermal efficiency of is less than 20% in theory because they are based on intrinsically irreversibly thermodynamic cycle. The Stirling-cycle based travelling wave thermoacoustic engines employ an inherently reversible thermodynamic cycle, and their thermal efficiency can reach up to 30% [2]. Increasing these efficiencies still proves a significant challenge to the research community. However, thermoacoustics is a new technology which holds a great promise of utilization of low-temperature or waste heat energy sources. Thermoacoustic devices can work with relatively low

Z. Yu and A. S. Abduljalil are with the School of Mechanical, Aerospace and Civil Engineering, University of Manchester, Sackville Street, PO Box 88, Manchester M60 1QD, UK. (e-mails: Zhibin.Yu@manchester.ac.uk and aalsayed@gmail.com respectively).

A. J. Jaworski, the corresponding author, is with the School of Mechanical, Aerospace and Civil Engineering, University of Manchester, Sackville Street, PO Box 88, Manchester M60 1QD, UK. (phone:+44(0)1612754352; fax: +44(0)8701307474; e-mail: a.jaworski@manchester.ac.uk).

temperature differences, and can be built using easily available materials without the need for highly skilled labour, all of which are great advantages for mass production. Furthermore, thermoacoustic devices can successfully compete with conventional energy-conversion technologies in situations where low cost and simplicity of construction are the main considerations.

It is well known that the standing wave thermoacoustic engine self-starts and maintains the acoustic oscillation, which converts heat energy to acoustic power, once the temperature gradient along the stack reaches the starting point, which is so-called onset temperature gradient [3]. In this respect, one of the critical issues is to decrease the thermoacoustic engine's onset temperature gradient ∇T_{onset}. Anthony [4, 5] carried out an analysis of the onset conditions in a standing wave thermoacoustic engine in terms of its quality factor Q, which is defined as

$$Q = -\omega \dot{E}_{st} / \dot{E}, \qquad (1)$$

where, $\dot{E}_{st}$ is the energy stored in the engine and can be obtained by integrating the time averaged acoustic energy density throughout the entire volume of the engine. $\dot{E}$ is the net power output of the entire engine, and can be expressed as

$$\dot{E} = \dot{E}_{stk} + \dot{E}_{HX} + \dot{E}_{res} \qquad (2)$$

where, the subscripts "stk", "HX" and "res" refer to the stack, the (hot and cold) heat exchangers and the resonator tube. $\dot{E}_{HX}$ and $\dot{E}_{res}$ are the dissipations in the heat exchangers and resonator tube, and are defined as negative. $\dot{E}_{stk}$ is essentially the "net" acoustic power out from the stack, and depends on the temperature gradient ∇T along the stack. There is a critical temperature gradient ∇T_{crit} for a stack [6,7] (when $\dot{E}_{stk} = 0$), so that $\dot{E}_{stk} < 0$ when $\nabla T < \nabla T_{crit}$, and $\dot{E}_{stk} > 0$ when $\nabla T > \nabla T_{crit}$.

Therefore, for a standing wave engine, as ∇T increases to ∇T_{crit} initially, the acoustic production in the stack overcomes the dissipation in the stack itself. At this point, $\dot{E}$ is still negative, and Q is still positive and finite. When ∇T increases to ∇T_{onset}, $\dot{E} = 0$ and Q is infinite, the net loss of the engine is zero, as a results, the engine reaches onset point. Above this point, any infinitesimal increase of ∇T will lead

World Academy of Science, Engineering and Technology
International Journal of Aerospace and Mechanical Engineering
Vol:3, No:1, 2009

to a negative Q and make the engine start the self-oscillation. Anthony [3] also performed the corresponding experimental measurement of the ∇T_{onset} of his standing wave thermoacoustic engine. The experimental results agree with the predicted ones very well.

Based on the above discussion, it can be found that ∇T_{onset} can possibly be decreased by two means: one is to reduce the dissipation in the heat exchanges ($\dot{E}_{HX}$) and the resonator tube($\dot{E}_{res}$); the other is to reduce ∇T_{crit} of the stack. Apparently, $\dot{E}_{HX}$ and $\dot{E}_{res}$ mainly depend on the roughness and the surface contact area with the working fluid, and so they can be reduced by improving the surface, however, this improvement is limited and costly. Another method is to reduce the critical temperature gradient of the stack.

In this paper, we will analyze the impact of the viscous dissipation and the heat relaxation loss in the stacks, as well as their impact on the critical temperature gradient ∇T_{crit} of the stack. The analysis assumes that the stack is short enough and does not alter the standing wave in an ideal gas where it is located. Based on the linear thermoacoustic theory, the energy flow within the stack is investigated, and a dimensionless critical temperature factor is obtained, which reveals the impact of the transverse dimensions of the channels, the local acoustic impedance of the stack, and the geometrical configuration of stack on the critical temperature gradient. The numerical analysis has been carried out to study the possible optimum combination between these parameters which leads to the lowest critical temperature gradient. Three different geometries, parallel plates, pin array, and circular pores, have been compared and discussed.

II. THEORETICAL ANALYSIS

According to the linear thermoacoustic theory [7], the time-averaged acoustic power $d\dot{E}_{stk}$ produced in a length dx of the channel can be written in the complex notation in the general form as

$$\frac{d\dot{E}_{stk}}{dx} = \frac{1}{2}\text{Re}\left[\tilde{U}_1 \frac{dp_1}{dx} + \tilde{p}_1 \frac{dU_1}{dx}\right], \quad (3)$$

where, U_1 and p_1 are complex volumetric velocity and pressure, respectively. "~" indicates a complex conjugate. $\text{Re}[\ ]$ denotes the real part of a complex number.

For regular geometries, f_v and f_k are functions of r_h/δ_k and have analytical formulae [7]. Therefore, equation (3) can be written as

$$\frac{d\dot{E}_{stk}}{dx} = -\frac{r_v}{2}|U_1|^2 - \frac{1}{2r_k}|p_1|^2 + \frac{1}{2}\text{Re}\left[g\tilde{p}_1 U_1\right]. \quad (4)$$

Viscous resistance per unit length of the channel, r_v, thermal-relaxation conductance per unit length of the channel, $1/r_k$,

and the complex gain/attenuation constant for the volume flow rate, g, are defined as follows:

$$r_v = \frac{\omega \rho_m}{A} \frac{\text{Im}\left[-f_v\right]}{|1-f_v|^2}, \quad (5)$$

$$\frac{1}{r_k} = \frac{\gamma-1}{\gamma} \frac{\omega A}{p_m} \text{Im}\left[-f_k\right], \quad (6)$$

and

$$g = \frac{(f_k - f_v)}{(1-f_v)(1-\sigma)} \frac{1}{T_m} \frac{dT_m}{dx}. \quad (7)$$

The Rott's functions f_v and f_k for selected regular geometries, can be found elsewhere [6, 7] in detail. γ, σ, ρ_m, p_m and T_m are the ratio of specific heat capacity, Prandtl number, mean density, mean pressure and mean temperature of the working gas, respectively.

On the right hand side (RHS) of equation (4), the first two terms represent viscous and thermal-relaxation dissipation, respectively, which always consume acoustic power, regardless of the temperature gradient along the length of the regenerator (or stack). The third term denotes the acoustic power produced (or consumed) by the regenerator due to the axial temperature gradient. It depends on the amplitude and direction of the axial temperature gradient. In engines, T_m increases in the direction of positive acoustic power flow, so the third term denotes the acoustic power produced from heat energy. For the refrigerators, T_m decreases in the direction of positive acoustic power flow, in which case the third term means the acoustic power consumed to pump heat from the cold to the hot end of the stack. This paper focuses only on the analysis of stacks in engines. Therefore, it will be more convenient to refer to $d\dot{E}_{stk}/dx$ as "net" time averaged acoustic power production per unit length of stack, because it is a net effect due to the acoustic power dissipation (the first two terms of the RHS of equation (4)) and the acoustic power production (the third term).

For an ideal standing wave, $\theta(p_1, U_1) = \pi/2$, and therefore,

$$\text{Re}\left[\tilde{p}_1 U_1\right] = 0, \quad (8)$$

and

$$\text{Im}\left[\tilde{p}_1 U_1\right] = |p_1||U_1|. \quad (9)$$

Substituting equations (8) and (9) into equitation (4), the following is obtained

$$\frac{d\dot{E}_{stk}}{dx} = \frac{1}{2}\left\{-r_v|U_1|^2 - \frac{1}{r_k}|p_1|^2 + \text{Im}[-g]|p_1||U_1|\right\} \quad (10)$$

Substituting (5), (6) and (7) into equation (10), the following relationship is obtained:

World Academy of Science, Engineering and Technology
International Journal of Aerospace and Mechanical Engineering
Vol:3, No:1, 2009

$$\frac{d\dot{E}_{stk}}{dx} = \frac{1}{2}\left\{-\frac{\omega\rho_m}{A}\frac{\text{Im}[-f_v]}{|1-f_v|^2}|U_1|^2 - \frac{\gamma-1}{\gamma}\frac{\omega A}{p_m}\text{Im}[-f_k]|p_1|^2\right.$$
$$\left.+\frac{1}{T_m}\frac{dT_m}{dx}\text{Im}\left[-\frac{(f_k-f_v)}{(1-f_v)(1-\sigma)}\right]|p_1||U_1|\right\} \quad (11)$$

Letting the RHS of equation (11) equate to zero, the following expression can be obtained for the critical temperature gradient for which $d\dot{E}_{stk}/dx = 0$.

$$\left(\frac{dT_m}{dx}\right)_{crit} = \frac{\frac{\omega\rho_m}{A}\frac{\text{Im}[-f_v]}{|1-f_v|^2}|U_1|^2 + \frac{\gamma-1}{\gamma}\frac{\omega A}{p_m}\text{Im}[-f_k]|p_1|^2}{\text{Im}\left[-\frac{(f_k-f_v)}{(1-f_v)(1-\sigma)}\right]|p_1||U_1|}T_m \quad (12)$$

Comparing equation (11) with equation (4), it can be found that the acoustic power produced in the stack due to the thermoacoustic process is dissipated by the viscous dissipation and the thermal relaxation dissipation when the temperature gradient through the stack is $\left(\dfrac{dT_m}{dx}\right)_{crit}$. Equation (12) takes into account both the viscous and thermal-relaxation dissipation. Therefore, it is a more general expression of the critical temperature gradient corresponding to $\dfrac{d\dot{E}_{stk}}{dx} = 0$ for stacks in a standing wave. For verification, neglecting the viscosity and setting $\sigma = 0$ and $f_v = 0$, equation (12) can be simplified to equation (13) given by Swift [7].

$$(dT_m/dx)_{crit} = \omega A|p_1|/\rho_m c_p|U_1| \quad (13)$$

To simplify this equation further, the local acoustic impedance will be introduced as

$$Z = \frac{p_1}{U_1}. \quad (14)$$

For the lossless planar standing wave, the acoustic impedance in equation (14) can be further defined as [7]

$$Z_{SW} = \frac{p_1}{U_1} = \frac{\rho_m a}{A}\tan\left(\frac{2\pi(x-x_0)}{\lambda}\right). \quad (15)$$

Here, x_0 indicates the position of the pressure node (and the volumetric velocity anti-node), and subscript "SW" refers to the standing wave. Substituting equation (15) into equation (12) leads to the following expression:

$$\left(\frac{dT_m}{dx}\right)_{crit} = \frac{\frac{\omega\rho_m}{A}\frac{\text{Im}[-f_v]}{|1-f_v|^2} + \frac{\gamma-1}{\gamma}\frac{\omega A}{p_m}\text{Im}[-f_k]\left(\frac{\rho_m a}{A}\right)^2\tan^2\left(\frac{2\pi(x-x_0)}{\lambda}\right)}{\text{Im}\left[-\frac{(f_k-f_v)}{(1-f_v)(1-\sigma)}\right]\frac{\rho_m a}{A}\tan\left(\frac{2\pi(x-x_0)}{\lambda}\right)}T_m \quad (16).$$

According to equation (15), $\tan\left(\dfrac{2\pi(x-x_0)}{\lambda}\right)$ is a dimensionless impedance factor. From equation (16), we can find that this dimensionless impedance factor actually controls the proportion between the viscous dissipation, thermal-relaxation dissipation, and acoustic power produced from heat energy through the thermoacoustic process. Furthermore, $\tan\left(\dfrac{2\pi(x-x_0)}{\lambda}\right)$ is a function of the stack location $(x-x_0)$. Therefore, equation (16) indicates a relationship between the critical temperature gradient and the location of the stack in the acoustic field.

Substituting equations (15) and (16) back into equation (11), the following relationship can be obtained:

$$\frac{d\dot{E}_{stk}}{dx} = \frac{1}{2}\frac{\omega A}{\gamma p_m}|p_1|^2\left(\frac{dT_m/dx}{(dT_m/dx)_{crit}}-1\right)$$
$$\left\{\text{ctan}^2\left(\frac{2\pi(x-x_0)}{\lambda}\right)\frac{\text{Im}[-f_v]}{|1-f_v|^2}+(\gamma-1)\text{Im}[-f_k]\right\} \quad (17)$$

From equation (17), it is easy to understand that a smaller $(dT_m/dx)_{crit}$ is also helpful to get a higher $d\dot{E}_{stk}/dx$ for a stack, which indicates the power production ability of the stack. For an easy verification, setting $f_v = 0$, equation (17) can be simplified to the equation given by Swift [7]:

$$\frac{d\dot{E}_{stk}}{dx} = \frac{1}{2}\frac{(\gamma-1)\omega A}{\gamma p_m}\text{Im}[-f_k]|p_1|^2\left(\frac{dT_m/dx}{(dT_m/dx)_{crit}}-1\right) \quad (18)$$

where, $(dT_m/dx)_{crit}$ is defined by equation (13).

Based on equation (16), the analysis of the critical temperature gradient can be continued. For ideal gases, the speed of sound $a = \sqrt{\gamma\Re T_m}$ ($\Re$ is the gas constant per unit mass), and the mean pressure $p_m = \rho_m\Re T_m$. In addition, $a = \omega\lambda/2\pi$, where λ is the wavelength. Thus, equation (16) can be simplified to:

$$\left(\frac{dT_m}{dx}\right)_{crit} = 2\pi\frac{\frac{\text{Im}[-f_v]}{|1-f_v|^2}+(\gamma-1)\text{Im}[-f_k]\tan^2\left(\frac{2\pi(x-x_0)}{\lambda}\right)}{\text{Im}\left[-\frac{(f_k-f_v)}{(1-f_v)(1-\sigma)}\right]\tan\left(\frac{2\pi(x-x_0)}{\lambda}\right)}\cdot\frac{T_m}{\lambda}. \quad (19)$$

Considering the dimensions of the RHS of equation (15), it can be found that $\dfrac{T_m}{\lambda}$ has the dimension of temperature gradient. Therefore, the remaining of the RHS of equation (19) is a dimensionless factor. For the convenience of the following discussion, we can define it as a dimensionless temperature gradient Θ_{crit}

$$\Theta_{crit} = 2\pi\frac{\frac{\text{Im}[-f_v]}{|1-f_v|^2}+(\gamma-1)\text{Im}[-f_k]\tan^2\left(\frac{2\pi(x-x_0)}{\lambda}\right)}{\text{Im}\left[-\frac{(f_k-f_v)}{(1-f_v)(1-\sigma)}\right]\tan\left(\frac{2\pi(x-x_0)}{\lambda}\right)} \quad (20)$$

Consequently,

World Academy of Science, Engineering and Technology
International Journal of Aerospace and Mechanical Engineering
Vol:3, No:1, 2009

$$\Theta_{crit} = \frac{(dT_m/dx)_{crit}}{T_m/\lambda} \ . \qquad (21)$$

According to equation (20), Θ_{crit} is a function of σ, γ, $(x-x_0)$, f_k and f_v. Furthermore, f_k and f_v are functions of r_h/δ_k and the geometrical configurations of the stack channels [6, 7]. Here, r_h is the hydraulic radius of the channel in the stack and defined as the ratio of the cross-sectional area A over perimeter $\prod$ [7]

$$r_h = \frac{A}{\prod} \ . \qquad (22)$$

Thermal penetration depth δ_k is defined as

$$\delta_k = \sqrt{2\kappa/\omega} \ , \qquad (23)$$

where, κ is the thermal diffusivity of working gas.

For a stack with given geometrical configuration, when the working gas is given, σ and γ are given, consequently, Θ_{crit} becomes a simple function of r_h/δ_k and $(x-x_0)$ only. In this respect, using equation (20), one can actually study the impact of geometrical configuration, r_h/δ_k and $(x-x_0)$ on the critical temperature gradient, as well as the optimum combination between these parameters.

III. NUMERICAL ANALYSIS AND DISCUSSION

To illustrate the application of the dimensionless factor Θ_{crit} obtained in Section II, numerical calculations for selected stack geometries: parallel-plate, pin-array and circular-pore, have been performed. The dimensionless transverse dimension of the channel, r_h/δ_k, was adopted for the stack calculations here. All calculations were performed for helium as the working fluid ($\sigma = 2/3$, $\gamma = 5/3$). The pin array used here has the same arrangement and dimension as that described by Hayden [9]. For the convenience of comparison, porosities are kept the same for the stacks (with different geometrical configuration) studied in the following calculations.

A. Parallel-Plate Stack

For the parallel-plate stack in the standing wave systems, according to equation (20), $(x-x_0)$ can be used as a factor indicating the local acoustic impedance. It represents the distance from the anti-node of velocity (or pressure node) to the position under study. Due to the function 'tan()' in equation (15) being periodic and odd, it is only necessary to study the range of $0 < 2\pi(x-x_0)/\lambda < \pi/2$, corresponding to $0 < (x-x_0) < \lambda/4$. For $-\lambda/4 < (x-x_0) < 0$, the negative sign only means the direction of the power flow.

Fig. 1 shows the results for the parallel-plate stack in the standing wave for different values of $(x-x_0)$. For each

value of $(x-x_0)$, Θ_{crit} firstly decreases sharply, and then increases slightly as r_h/δ_k increases. There is a minimum Θ_{crit} when r_h/δ_k varies in the tested range. This minimum Θ_{crit} is denoted as $(\Theta_{crit})_{min}$. It also corresponds to a value of r_h/δ_k which is referred as $(r_h/\delta_k)_{opti}$.
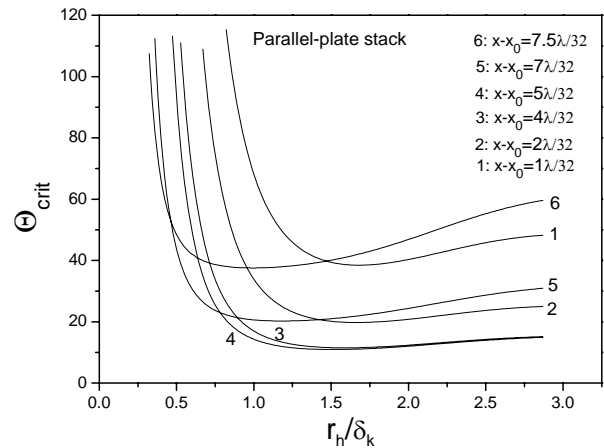

Fig. 1 Parallel-plate stack in the standing wave: the calculated value of Θ_{crit} versus r_h/δ_k for different locations. For each $(x-x_0)$, there is a minimum value of Θ_{crit} when r_h/δ_k varies

According to the derivation in section II, dimensionless critical temperature gradient factor Θ_{crit} directly reflects the critical temperature gradient of the tested stack. Therefore, the results shown in Fig. 1 reveal that both the location of the stack and the transverse dimension of the channel significantly affect the critical temperature gradient. When $r_h < \delta_k$ (i.e. $r_h/\delta_k < 1$), the value of r_h/δ_k strongly impacts the critical temperature gradient. A smaller value of r_h/δ_k will lead to a higher critical temperature gradient. This is because that, in this range of r_h/δ_k, the viscous dissipation dominates in the stack compared with the thermal relaxation dissipation. A relatively smaller channel size means higher viscous dissipation for a given operating condition.

However, for the right branch of each curve in Fig. 1 (i.e. when $r_h > \delta_k$), the channel size is relatively large, thus the thermal relaxation dissipation in the stack is dominant compared to the viscous dissipation. Furthermore, the thermal relaxation dissipation mainly depends on the magnitude of δ_k. Therefore, as the channel size increases (i.e. r_h/δ_k increases), the critical temperature gradient increases only slightly (as shown in Fig. 1).

On the other hand, in Fig. 1, one can also find that $(\Theta_{crit})_{min}$ and $(r_h/\delta_k)_{opti}$ vary as the value of $(x-x_0)$ varies. This is due to that $\tan\left(\dfrac{2\pi(x-x_0)}{\lambda}\right)$ varies when

World Academy of Science, Engineering and Technology
International Journal of Aerospace and Mechanical Engineering
Vol:3, No:1, 2009

$(x - x_0)$ varies which changes the proportion between the acoustic power dissipations and production. For further investigation, the additional information can be obtained by interpreting Fig. 1 as a graph of $(\Theta_{crit})_{\min}$ and $(r_h/\delta_k)_{opti}$ as a function of $(x - x_0)$ shown by solid lines in Fig. 2 and Fig. 3.

In Fig. 2, the solid line shows the relationship between $(\Theta_{crit})_{\min}$ and $(x - x_0)$ for tested parallel-plate stack. It can be seen that $(\Theta_{crit})_{\min}$ firstly decreases, and then increases as $(x - x_0)$ increases. The results show that the location of the stack strongly influences the critical temperature gradient. According to equation (15), smaller $(x - x_0)$ (i.e. close to the anti-node of velocity) leads to smaller $\tan\left(\dfrac{2\pi(x - x_0)}{\lambda}\right)$, thus, viscous dissipation dominates for the left branch in Fig. 2. Conversely, thermal-relaxation dissipation dominates for the right branch where the stack location is close to the node of velocity. Therefore, locating the stack to either node or anti-node of velocity will lead to a high critical temperature gradient.

Furthermore, in Fig. 2, $(\Theta_{crit})_{\min}$ reaches the lowest value when $(x - x_0) \approx 5\lambda/32$. Qualitatively, in the practical standing wave thermoacoustic engines with parallel-plate stacks, there exists an optimal region to locate the stack, about $\lambda/8 \sim 5\lambda/32$ away from the nearest velocity anti-node. In this situation, the engine has the lowest starting conditions.
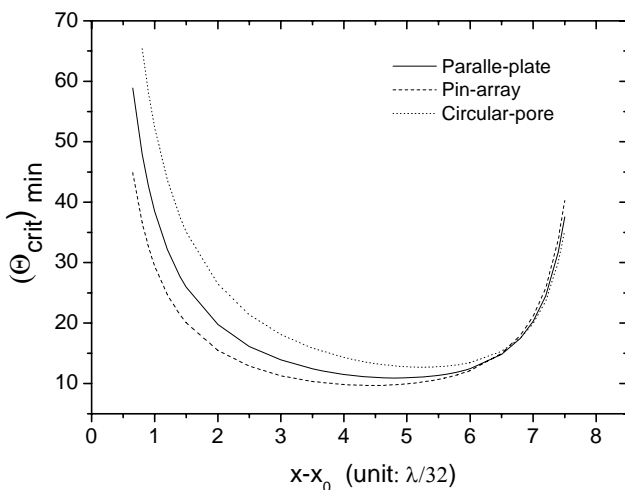

Fig. 2 The relationships of $(\Theta_{crit})_{\min}$ versus $(x - x_0)$ for the tested stacks with selected geometries. Solid line: parallel-plate; dashed line: pin-array; dotted line: circular-pore
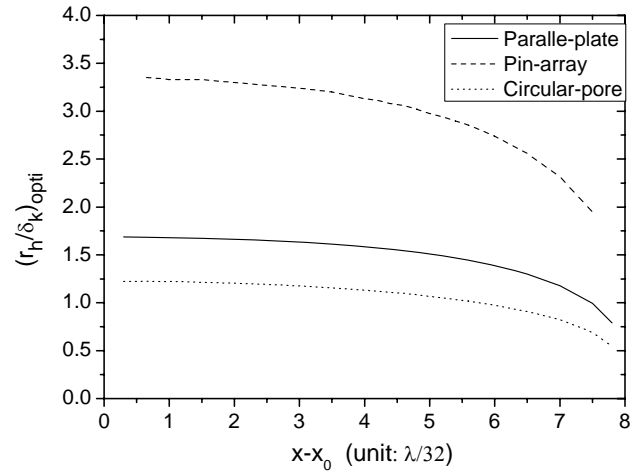

Fig. 3 The relationships of $(\delta_k/r_h)_{opti}$ versus $(x - x_0)$ for the tested stacks with selected geometries. Solid line: parallel-plate, Dashed line: pin-array, Dotted line: circular-pore

In Fig. 3, the solid line shows the relationship between $(r_h/\delta_k)_{opti}$ and $(x - x_0)$ for tested parallel-plate stack. It can be seen that $(r_h/\delta_k)_{opti}$ decreases from 1.6 to 0.8 as $(x - x_0)$ increases in the tested range. This is because $\tan\left(\dfrac{2\pi(x - x_0)}{\lambda}\right)$ increases as $(x - x_0)$ increases, and then changes the proportion of the three terms in the numerator and denominator of equation (20). The physics behind this figure is that, as $(x - x_0)$ increases, the $|U_1|$ decreases and $|p_1|$ increases, accordingly, the thermal-relaxation dissipation becomes more significant in the stack gradually. As a result, the corresponding optimal channel size (i.e. r_h here) decreases to keep the balance between these effects.

B. Comparison between Common Regular Geometries

Using the same methodology as in section III.A, one can perform a similar numerical analysis for pin-array and circular-pores stacks. Obtaining similar results to those shown in Figs. 1-3 is relatively straightforward for these two geometrical configurations and is shown in Figs. 2-4.

Fig. 4 is an example of this comparison for a given $(x - x_0) = 5\lambda/32$, of which the solid, dashed and dotted lines show the relationship between Θ_{crit} and r_h/δ_k for parallel-plate, pin-array and circular-pores, respectively. Fig. 4 shows that the three curves have similar shape, which reveals that r_h/δ_k impacts Θ_{crit} of stacks with these three geometrical configurations in a similar way.
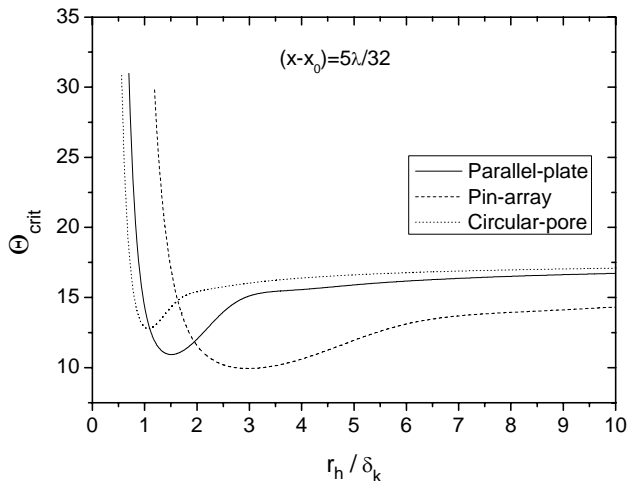
World Academy of Science, Engineering and Technology
International Journal of Aerospace and Mechanical Engineering
Vol:3, No:1, 2009

Fig. 4 For a given location, $(x - x_0) = 5\lambda/32$, the comparison of the relationship between Θ_{crit} and r_h/δ_k. Solid line: parallel-plate, Dashed line: pin-array, Dotted line: circular-pore.

In Fig. 2, the dashed and dotted lines show the results of the tested pin-array and circular-pore stacks, respectively. They have quite similar shapes to those of parallel-plate stack. Fig. 2 also shows that $(\Theta_{crit})_{min}$ for the tested pin-array stack is below those for the tested parallel-plate stack. However, the $(\Theta_{crit})_{min}$ for the tested circular-pore stack are above those. Furthermore, the differences of $(\Theta_{crit})_{min}$ between different geometries becomes bigger when stack location approaches to the anti-node of velocity (i.e. $(x - x_0) \to 0$), and smaller when approaches to node of velocity (i.e. $(x - x_0) \to \lambda/4$). If $(\Theta_{crit})_{min}$ is regarded as a quality indicator of the stack with the geometries tested, the results in Fig. 2 reveal that performance difference of the stack depends on the location of the stack in the standing-wave acoustic field (in other words, depends on the local impedance).

Similarly, Fig. 3 shows the comparison of $(r_h/\delta_k)_{opti}$ for the stack stack geometries tested. The dashed and dotted lines show the results of the pin-array and circular-pore stacks, respectively. The lines have quite a similar shape to that for the parallel-plate stack. In a similar way, $(r_h/\delta_k)_{opti}$ decreases as $(x - x_0)$ increases in the tested range. The physics behind these curves are the same as those mentioned for parallel-plate stack. Furthermore, the difference in obtained $(r_h/\delta_k)_{opti}$ is mainly due to the definition of r_h for different geometries.

As discussed above, Fig. 2 shows the optimal performance, obtained by choosing the optimum combination between the transverse dimension of channels and the local acoustic impedance of stacks. We can continue the comparison in the region of our interest, $2\lambda/32 < (x - x_0) < 6\lambda/32$. For convenience, the results for circular-pore stack are used as a benchmark. The results for the stacks with two other geometries are normalized by dividing by those for the circular-pore stack. Such a comparison is shown in Fig. 5, where the solid and dashed lines show the normalized $(\Theta_{crit})_{min}$ for the pin-array and parallel-plate stacks, respectively. It can be found that, $(\Theta_{crit})_{min}$ for the pin-array stack is about 46% less than that of the circular-pore stack when $(x - x_0) = 2\lambda/32$. As $(x - x_0)$ increases, the difference decreases to about 10% at $(x - x_0) = 6\lambda/32$. Similarly, $(\Theta_{crit})_{min}$ for the circular-pore stack is about 36% bigger than that of parallel-plate stack when $(x - x_0) = 2\lambda/32$, the difference decreases to about 7.5% at $(x - x_0) = 6\lambda/32$.
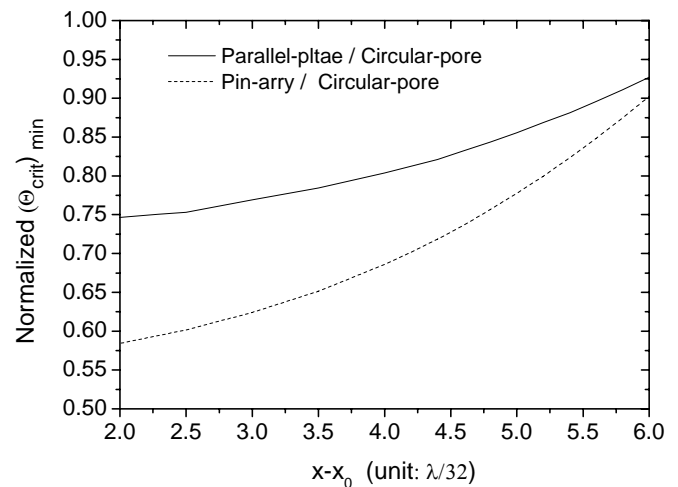

Fig. 5 Comparison between the pin-array, parallel-plate and circular-pore stacks. The results for the circular-pore stack are used as the reference for the normalization

To compare different stacks in standing-wave thermoacoustic systems, Swift et al. [8] defined a tentative figure of merit $M = \sqrt{\sigma} \, \text{Im}[f_k] |1 - f_v|^2 / \text{Im}[f_v]$, based on the idea that the thermoacoustic heat transport and work are proportional to $\text{Im}[f_k]$ in the standing wave, inviscid limit, and that the acoustic power dissipated by viscosity is proportional to $\text{Im}[f_v]/|1 - f_v|^2$ when $dT_m/dx = 0$. Furthermore, $\tilde{M}$ is defined as the value of M when $\text{Im}[f_k]$ is maximum [8]. Based upon this simplified criterion, the optimum pin-array stack is 23% more efficient than the optimum parallel-plate stack operating at the same gas pressure and frequency, and 51% more efficient than the optimum circular-pore stack [9].

Using the method in this paper, $\tan\left(\dfrac{2\pi(x - x_0)}{\lambda}\right) = 1$ when $(x - x_0) = 4\lambda/32$, then the impedance factor vanishes in equation (20). This case is equivalent to the comparison using

$M = \sqrt{\sigma}\,\text{Im}[f_k]\left|1 - f_v\right|^2 / \text{Im}[f_v]$ which does not consider the effect of the local acoustic impedance of stack. In this case, $(\Theta_{crit})_{min}$ of the pin-array and parallel-plate stack are about 35% and 20% less than that of the circular-pore stack. It can be found that, although the comparisons are based on two different methods, they qualitatively agree with each other.

IV. CONCLUSION

Based on the assumptions of a standing wave in ideal gas, a dimensionless factor Θ_{crit} has been obtained to evaluate the critical temperature gradient of stacks in the standing wave thermoacoustic engines. This factor can clearly reveal the relationship between the channel dimension, impedance, geometries and the critical temperature gradient.

It is shown that the local acoustic impedance of the stacks essentially represents the proportion between the acoustic power produced from the heat energy through the thermoacoustic processes and the acoustic power dissipated by viscous and thermal-relaxation effects in the stacks. The critical temperature gradient is strongly dependent on the impedance. Locating the stack close to either the anti-node or node of velocity will lead to high critical temperature gradient, which reflects the onset condition in practical standing wave thermoacoustic engines. Therefore, the local acoustic impedance has to be taken into account for any evaluation of stacks, as well as the comparison between different geometrical configurations or dimensions.

The numerical results also indicate that the channel dimension affects the critical temperature gradient of stacks (see Figs. 1 and 4). Theoretically, for the stacks, the optimum transverse dimension of the channel exists, but depends on the local acoustic impedance. Therefore, to get the lowest critical temperature gradient, the stacks can be optimized by choosing an optimum combination between the transverse dimension of the channel and impedance (for example: $(x - x_0) \approx 5\lambda/32$, and $r_h/\delta_k = 1.5$ for parallel-plate stack). However, it is also shown that the optimal range of impedance is broad as shown in Fig. 2.

The comparison of critical temperature gradient has been performed using the defined dimensionless factor for the stack with three commonly used geometries. It is indicated that geometries significantly affect the critical temperature gradient, pin-array being best, parallel-plat being medium, and circular-pore being worst of the three. However, the difference depends on the local impedance as shown in Figs. 2 and 5.

Although all the calculations are performed for helium, the general principles are valid for other working gases. The Prandtl number σ and the ratio of specific heat capacities γ are simply additional parameters in equation (20). The calculations shown in this paper are applicable for pure monatomic gases. For polyatomic gases, such as nitrogen, $\gamma = 7/5$ could be used, but the results are quite similar to those for helium.

REFERENCES

[1] G. W. Swift, "Analysis and performance of a large thermoacoustic engine", *J. Acoust. Soc. Am.*, vol. 92, no. 3, pp. 1551-1563, Sept. 1992.
[2] S. Backhaus and G. W. Swift, "A thermoacoustic-Stirling heat engine: Detailed study", *J. Acoust. Soc. Am.*, vol. 107, pp. 3148-3166, June, 2000.
[3] A. A. Atchley, F.M. Kuo, "Stability curves for a thermoacoustic prime mover", *J. Acoust. Soc. Am.*, vol. 95, no. 3, pp. 1401-1404, March, 1994.
[4] A. A. Atchley, "Standing wave analysis of a thermoacoustic prime mover below onset of self-oscillation", *J. Acoust. Soc. Am.* vol. 92, no. 5, pp. 2907-2914, Nov., 1992.
[5] A. A. Atchley, "Analysis of the initial buildup of the oscillations in a thermoacoustic prime mover", *J. Acoust. Soc. Am.*, vol. 95, no. 3, pp. 1661-1664, March, 1994.
[6] G. W. Swift, "Thermoacoustic engines", *J. Acoust. Soc. Am.*, vol. 84, no. 4, pp. 1145–1180, Oct., 1988.
[7] G. W. Swift, *Thermoacoustics: A Unifying Perspective for some Engines and Refrigerators.* Acoustical Society of America, Sewickley PA, 2002, ch. 4.
[8] G. W. Swift, and R. M. Keolian, "Thermoacoustics in pin-array stacks", *J. Acoust. Soc. Am.*, vol. 94, no. 2, pp941-943, Aug., 1993.
[9] M.E. Hayden and G. W. Swift, "Thermoacoustic relaxation in a pin-array stack", *J. Acoust. Soc. Am.*, vol. 102, no. 5, pp. 2714-2722, Nov. 1997.